SCIENCE CHINA
Information Sciences

• Supplementary File •

Doping and minority carrier lifetime uniformity of 4H-SiC homoepitaxial layers: Role of C/Si Ratio Distribution

Wenji Liu[1,2], Zhouyu Tong[1,2], Cong Zhang[1,2], Xuefeng Han[1,2], Rong Wang[1,2*], Deren Yang[1,2] & Xiaodong Pi[1,2*]

[1]*State Key Laboratory of Silicon and Advanced Semiconductor Materials & School of Materials Science and Engineering, Zhejiang University, Hangzhou 310027, China*
[2]*Institute of Advanced Semiconductors & Zhejiang Provincial Key Laboratory of Power Semiconductor Materials and Devices, Hangzhou Innovation Center, Zhejiang University, Hangzhou 311200, China*

Appendix A Simulation model and equations

The numerical simulation was performed using the commercial software COMSOL Multiphysics, which couples the electromagnetic heating, non-isothermal flow, and reaction kinetics. To facilitate simulation, the graphite supporting structure and cover plate were simplified. The density of the mesh is refined at the reaction surface so that the solutions are grid independent. During the hot-wall CVD, 4H-SiC substrates are placed in the gas channel formed by top and bottom graphite susceptors. Upon heating, 4H-SiC wafers are heated from both sides, which are thermal radiation from the top graphite susceptor and thermal conduction/radiation from the back graphite. It has been demonstrated that the temperature gradient inside the 150 mm wafer is as low as 0.02 K/mm [1]. Therefore, the temperature distribution on the 4H-SiC substrate is considered as uniform. Given the typical dimensionless numbers during the CVD process, gas flow was assumed to be compressible and laminar. It was assumed that the gas has enough time to form the stable laminar flow before entering the susceptor, the flow is thus not affected by the shortening of the gas inlet. The main coupled equations for the numerical simulation are [2,3]:

$$\rho C_p u \cdot \nabla T + \nabla \cdot q = Q + Q_p + Q_{vd}, \tag{A1}$$

$$q = -k\nabla T, \tag{A2}$$

$$\nabla \cdot J_i + u \cdot \nabla c_i = R_i, \tag{A3}$$

$$J_i = -D_i \nabla c_i, \tag{A4}$$

where ρ is the mass density of gas mixture from the equation of state of ideal gas, u is the vector of mass average velocity, and p is the pressure. T is the temperature, R_i is the reaction rate, D_i is the gas diffusivity, Q is the external heat sources, C_p is the heat capacity, and k is the thermal conductivity. Subscript i denotes the ith gas species.

Appendix B Reaction kinetics

There are large number of possible reaction steps in the TCS-C_2H_4-H_2 system, and incorporating all of them in the model is impossible. Therefore, molecules containing more than four carbon (or four silicon) atoms and molecules with fewer carbon (or silicon) atoms, whose concentrations are too low, are not taken into account during the simulations. All of the molecules excluded from the model are produced in very small quantities under normal 4H-SiC CVD conditions [4,5], so they would not significantly contribute to epitaxy of 4H-SiC. The reaction kinetics with the reaction rate constants are listed in Table 1 [6–9]. The rate constants are written according to Arrhenius equation in units consistent with m, s, and mol, and the activation energies in J/mol.

* Corresponding author (email: rong_wang@zju.edu.cn, xdpi@zju.edu.cn)

Table B1 List of main gas-phase reactions during the epitaxy of 4H-SiC.

No.	Reactions	A	n	E
1	$C_2H_4 \rightarrow C_2H_2 + H_2$	5.32×10^{11}	0.89	4.55×10^5
	Reverse rate	4.32×10^2	1.27	2.71×10^5
2	$C_2H_4 \rightarrow C_2H_3 + H$	4.37×10^{12}	0.95	4.52×10^5
	Reverse rate	8.43×10^7	0	0
3	$2C_2H_4 \rightarrow C_2H_3 + C_2H_5$	4.82×10^8	0	2.99×10^5
	Reverse rate	4.82×10^5	0	0
4	$C_2H_4 \rightarrow C_2H_5 + H$	1.02×10^7	0	2.85×10^5
	Reverse rate	1.81×10^6	0	0
5	$C_2H_5 \rightarrow C_2H_4 + H$	1.66×10^{13}	0.09	1.72×10^5
	Reverse rate	9.83×10^7	0.10	3.01×10^4
6	$C_2H_5 + H_2 \rightarrow C_2H_6 + H$	3.07×10^{-6}	3.60	3.50×10^4
	Reverse rate	1.45×10^3	1.50	3.10×10^4
7	$C_2H_5 + C_2H_4 \rightarrow C_2H_6 + C_2H_3$	6.62×10^{-4}	3.13	7.54×10^4
	Reverse rate	6.02×10^{-4}	3.30	4.39×10^4
8	$C_2H_6 \rightarrow 2CH_3$	1.20×10^{22}	-1.79	3.81×10^5
	Reverse rate	1.02×10^9	-0.64	0
9	$C_2H_3 + H_2 \rightarrow C_2H_4 + H$	3.01×10^{-2}	2.63	3.60×10^4
	Reverse rate	1.33	2.53	5.10×10^4
10	$SiHCl_3 + H_2 \rightarrow SiH_2Cl_2 + HCl$	3.28×10^{-8}	4.22	2.33×10^5
	Reverse rate	3.82×10^{-5}	3.11	1.76×10^5
11	$SiHCl_3 + HCl \rightarrow SiH_4 + H_2$	2.20×10^{-3}	2.67	1.78×10^5
	Reverse rate	6.80	2.11	2.54×10^5
12	$SiHCl_3 \rightarrow SiHCl_2 + Cl$	3.50×10^{20}	-1.30	4.62×10^5
	Reverse rate	3.40×10^8	-0.12	-8.40×10^2
13	$SiHCl_2 + HCl \rightarrow SiHCl_3 + H$	2.40×10^{-4}	3.00	5.02×10^4
	Reverse rate	4.70×10^3	1.48	8.40×10^4
14	$SiHCl_2 + HCl \rightarrow SiH_2Cl_2 + Cl$	1.31×10^{-3}	3.03	2.68×10^4
	Reverse rate	2.34×10^{-7}	4.55	4.08×10^4
15	$SiH_2Cl_2 \rightarrow SiHCl + HCl$	6.92×10^{14}	0	3.17×10^5
	Reverse rate	1.71×10^3	0.91	4.60×10^4
16	$SiH_2Cl_2 \rightarrow SiCl_2 + H_2$	2.14×10^{18}	-1.20	3.26×10^5
	Reverse rate	9.41×10^{-17}	6.37	1.13×10^5
17	$SiCl_2 + HCl \rightarrow SiHCl_2 + Cl$	1.20×10^{-3}	2.95	2.44×10^5
	Reverse rate	1.49×10^{-2}	2.72	6.40×10^3
18	$SiCl_3 + H_2 \rightarrow SiHCl_2 + HCl$	3.99×10^{-8}	4.10	1.74×10^5
	Reverse rate	9.97	1.45	1.38×10^5
19	$SiCl_2 + H_2 \rightarrow SiHCl_2 + H$	1.10×10^{-3}	3.21	2.06×10^5
	Reverse rate	1.10×10^{-5}	1.15	-1.92×10^4
20	$SiH_2Cl_2 \rightarrow SiHCl_2 + H$	8.70×10^{17}	-0.70	3.89×10^5
	Reverse rate	1.40×10^7	0.18	-1.67×10^3
21	$SiHCl + HCl \rightarrow SiHCl_2 + H$	0.10	2.22	9.22×10^4
	Reverse rate	3.40×10^9	-0.61	5.20×10^3
22	$SiH_3Cl \rightarrow SiHCl + H_2$	3.89×10^{14}	2.00	2.72×10^5
	Reverse rate	2.63×10^8	0	7.60×10^4
23	$SiCl_4 \rightarrow SiCl_3 + Cl$	4.79×10^{15}	0	4.65×10^5
	Reverse rate	9.01×10^6	0.23	-1.67×10^3
24	$SiCl_4 + SiCl_2 \rightarrow 2SiCl_3$	2.66×10^{-9}	4.88	1.62×10^5
	Reverse rate	1.41×10^4	0.58	2.65×10^4

Appendix C Nitrogen distribution

3D simulations of the 4H-SiC CVD reactor, including inductive heating and fluid dynamics as well as gas phase and surface chemistry, is then performed to explain the deteriorative doping uniformity with higher inlet C/Si ratios. As shown in Figure C1, the nitrogen (N) concentration gradually increases along the direction of gas flow.Figure C1(a-c) shows the simulation results when the substrate is not rotating. Considering the rotation of the 4H-SiC substrate during the CVD process, Figure C1(d) presents the averaged N concentration at the same radius. As shown in Figure C1, the nonuniformity of the wafer-scale distribution of N concentration increases from 1.1% to 26.9% as the inlet C/Si ratio increases from 1.32 to 1.52. The "⋂"-shaped net carrier distribution under different inlet C/Si ratios is caused by the low doping species at the upstream of the reactor. In addition, the site competition effect indicates that the distribution of C/Si ratio also affects the distribution of doping concentration.

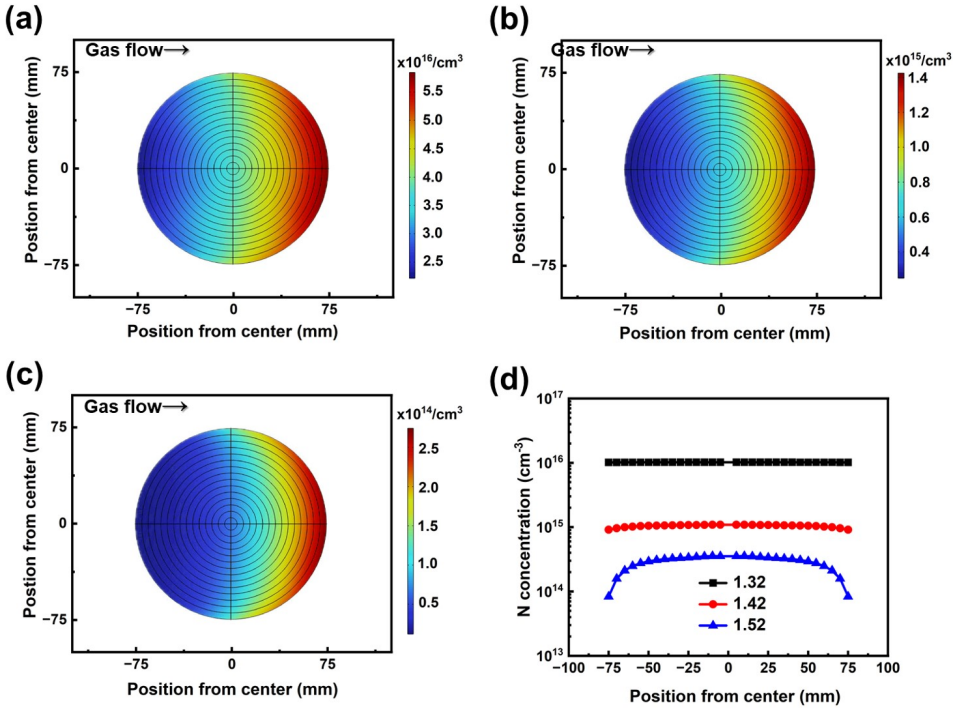

Figure C1 Simulations of the distribution of N concentration of 4H-SiC epitaxial layers under the inlet C/Si ratios of (a) 1.32, (b) 1.42, and (c) 1.52. (d) shows the radial distribution of N concentration under different inlet C/Si ratios.

Appendix D Minority carrier lifetime

In order to explain the deteriorative doping uniformity with higher inlet C/Si ratios, as well as the difference between experimental and simulation results, we investigate the effect of wafer-scale C/Si ratio on the doping uniformity. Because the minority carrier lifetime is closely related to the concentration of V_C [10], and thus related to the C/Si ratio, we then investigate the wafer-scale distribution of minority carrier lifetime of 4H-SiC under different inlet C/Si ratios. As shown in Figure D1, the minority carrier lifetime maximum increases from 450 ns to 1080 ns as the inlet C/Si ratio increases from 1.32 to 1.52. The deviation of minority carrier lifetime is 4.4%, 15.5% and 40.2% under the inlet C/Si ratio of 1.32, 1.42 and 1.52, respectively. Furthermore, the wafer-scale distribution of minority carrier lifetime exhibits the "M" and "⋂" shape under the inlet C/Si ratio of 1.32 (or 1.42) and 1.52, respectively.

Appendix E Temperature distribution

As shown in Figure E1, simulations of the thermal field indicate a temperature gradient of approximately 30 K/mm within the reaction chamber. This gradient is a key factor influencing the uniformity of the surface C/Si ratio. The calculations suggest that reducing the distance between the upper and lower horizontal hot walls can effectively decrease the gas temperature gradient, which in turn helps improve both the uniformity of the surface C/Si ratio and the doping uniformity simultaneously. The nonuniformity of the surface C/Si ratio increases as the height of the hot walls rises. When the hot wall height reaches 40 mm, the deviation in the surface C/Si ratio can be as high as 10.1%. However, if the hot wall height is too low, it may introduce uncontrollable factors such as turbulence, which can be detrimental to the epitaxial process.

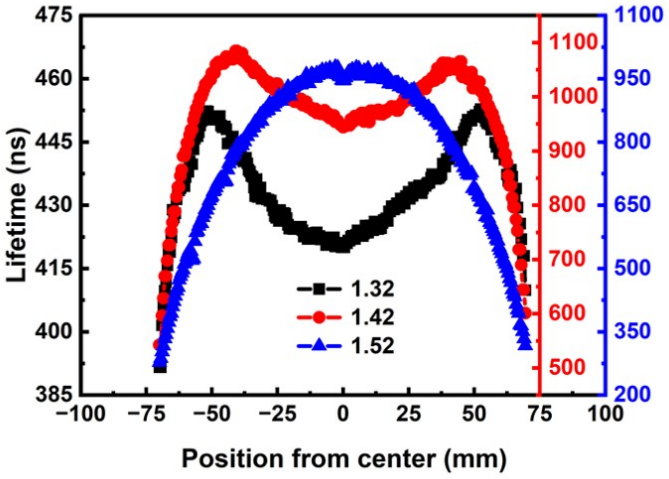

Figure D1 The radial distribution of minority carrier lifetime under different C/Si ratios.

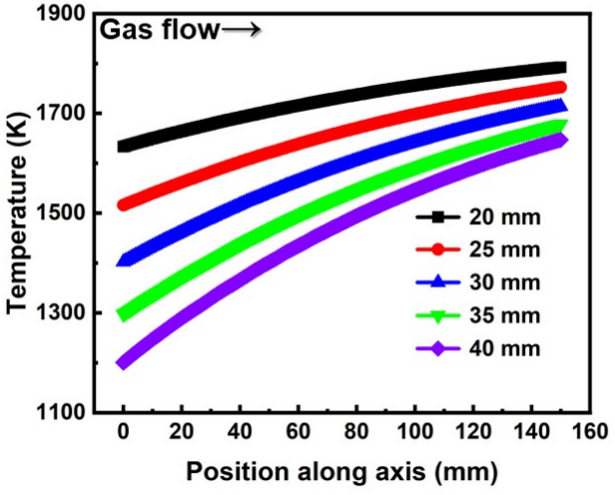

Figure E1 The distribution of gas temperature along the gas flow direction at half the hot-wall height above the substrate under different hot wall heights

Appendix F Surface C/Si distribution

Since the minority carrier lifetime of n-type 4H-SiC epitaxial layers is mainly determined by the concentrations of VC and N [10]. The surface C/Si ratio is then simulated to explain the variations in wafer-scale distribution of doping concentration and minority carrier lifetime. Because the carrier gas flow rate is much higher than that of the precursor flow rate, we assume that the flow field and thermal field remain unchanged when the inlet C_2H_4 flux decreases. We find that the surface C/Si ratio gradually decreases along the direction of gas flow, which results in a radial nonuniformity of the surface C/Si ratio during the epitaxy process.As shown in Figure F1, with the inlet C/Si ratio increases, the region close to the stoichiometric ratio moves to the outlet. Considering the substrate rotation, the wafer-scale distribution of C/Si ratio exhibits the same "$\cup$" shape under different inlet C/Si ratios. As the inlet C/Si ratio increases, the overall surface C/Si ratio increases. Therefore, the region with the stoichiometric ratio moves towards the wafer center, because of the increase of the C/Si ratio.

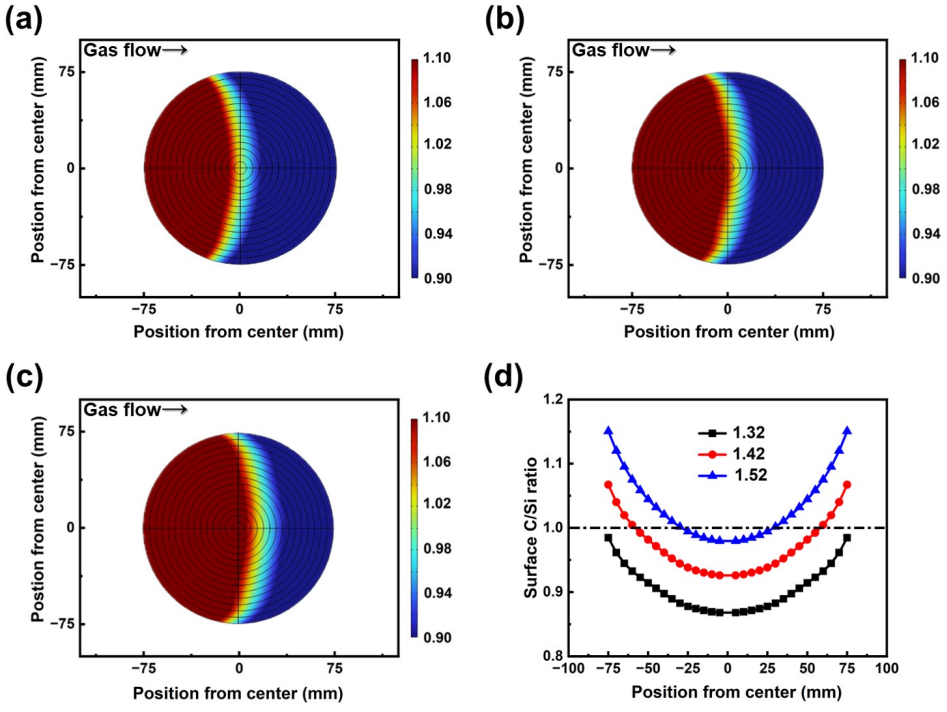

Figure F1 Simulated surface C/Si ratio distribution under the inlet C/Si ratios of (a) 1.32, (b) 1.42, and (c) 1.52. (d) shows the radial distribution of the surface C/Si ratios under different inlet C/Si ratios. The horizontal dashed line indicates the surface C/Si ratio of 1.

References

1 Danielsson Ö, Karlsson M, Sukkaew P, Pedersen H, Ojamaë L. A Systematic Method for Predictive in Silico Chemical Vapor Deposition. J Phys Chem C, 2020, 124: 7725–7736.
2 Song B, Gao B, Han P, Yu Y. Surface Kinetic Mechanisms of Epitaxial Chemical Vapour Deposition of 4H Silicon Carbide Growth by Methyltrichlorosilane-H2 Gaseous System. Materials (Basel), 2022, 15: 3768.
3 Li Q, Zhang Y, Ji B, Zhang S, Tu R. Improvement of SiC deposition uniformity in CVD reactor by showerhead with baffle. J Cryst Growth, 2023, 615: 127255.
4 Wang R, Ma R. Kinetics of halide chemical vapor deposition of silicon carbide film. J Cryst Growth, 2007, 308: 189–197.
5 Guan K, Gao Y, Zeng Q et al. Numerical modeling of SiC by low-pressure chemical vapor deposition from methyltrichlorosilane. Chinese J Chem Eng, 2020, 28: 1733–1743.
6 Nishizawa SI, Pons M. Growth and doping modeling of SiC-CVD in a horizontal hot-wall reactor. Chem Vap Depos, 2006, 12: 516–522.
7 Ravasio S, Masi M, Cavallotti C. Analysis of the gas phase reactivity of chlorosilanes. J Phys Chem A, 2013, 117: 5221–5231.
8 Veneroni A, Masi M. Gas-phase and surface kinetics of epitaxial silicon carbide growth involving chlorine-containing species. Chem Vap Depos, 2006, 12: 562–568.
9 Meziere J, Ucar M, Blanquet E et al. Modeling and simulation of SiC CVD in the horizontal hot-wall reactor concept. J Cryst Growth, 2004, 267: 436–451.
10 Kimoto T, Niwa H, Okuda T et al. Carrier lifetime and breakdown phenomena in SiC power device material. J Phys D Appl Phys, 2018, 51: aad26a.